Int J Adv Manuf Technol (2017) 93:3907–3920
DOI 10.1007/s00170-017-0756-5

ORIGINAL ARTICLE

# Noncontact measurements of acoustic emissions from the single-point turning process

**Peter L. Schmidt**[1] · **Jameson K. Nelson**[2] · **Rodney G. Handy**[3] · **Jonathan S. Morrell**[4] · **Mark J. Jackson**[2] · **Tracy M. Rees**[3]

Received: 11 November 2016 / Accepted: 26 June 2017 / Published online: 31 July 2017


**Abstract** Single-point turning is a fabrication process that is fundamental to manufacturing, comprising a significant portion of value-added operations. Vibration at the tool/workpiece interface affects surface finish, residual stress, and chemical reactivity of machined components. This phenomenon also affects tool life and therefore production cost. The study and measurement of this phenomenon has traditionally been done using a transducer in contact with the cutting tool or is in line with the cutting tool/tool holder assembly. While this setup has been acceptable for laboratory studies, implementation on actual production platforms has not been widespread, with open loop machine tool parameter control still being the norm. The goal of this study involves the use of a noncontact transducer (microphone) to gauge detectability and measurability of machine tool vibration attributable to the single-point turning process performed on a manual lathe situated in a shop floor environment. Such measures as characterization of the frequency content transmitted and the sound pressure level measured while machining a group of materials of interest are quantified and discussed. The results of the work show that the acoustic energy attributable to single-point turning is detectable using the noncontacting sensor, producing energy mostly in the ultrasonic ($f > 20$ kHz) range. Individual materials of interest (M42 tool steel, tungsten tantalum alloy, aluminum 6061, and Nitronic 33 stainless steel) are shown to emit distinct frequency signatures when excited using identical process parameters. Potential sources of ultrasonic acoustic emission are postulated and discussed, along with control of the turning process using the acoustic signal as an input and selected process parameter changes as the output.

**Keywords** Ultrasonic · Microphone · Vibration · Acoustics · Turning

✉ Peter L. Schmidt
ps125@evansville.edu

[1] Department of Mechanical and Civil Engineering, University of Evansville, 1800 Lincoln Avenue, Koch Center 269, Evansville, IN 47722, USA

[2] Center for Advanced Manufacturing, Purdue University, West Lafayette, IN 47907, USA

[3] Department of Family & Preventive Medicine, University of Utah, Salt Lake City, UT 84108, USA

[4] Electric Power Research Institute, Knoxville, TN 37932, USA

## 1 Introduction

### 1.1 Background

Single-point turning is a fabrication process that is fundamental to manufacturing, comprising a significant portion of value-added operations [1]. Material removal rates in turning operations are limited by the onset of instability at the tool/workpiece interface, commonly termed "chatter" [2]. This phenomenon has been exhaustively studied, with both analytical and empirical relationships in place to predict the onset of this condition [3–7]. Prudent manufacturers set process parameters to assiduously avoid having the chatter phenomenon affect the quality of their work product while maximizing cutting tool life. Use of analytical or empirical relationships in a closed loop control system relies on the implementation of a sensor system capable of monitoring this phenomenon in real time and providing feedback to some sort of control device or interface with a programmable machine tool [8, 9].

Sensor systems normally used to measure and study this phenomenon include an instrumented platform for holding the cutting tool and accelerometers measuring vibration in three

orthogonal axes. This instrumentation is expensive, especially if it is designed to operate in the harsh environment of flowing cutting fluid. The additional hardware in this system also introduces stiffness and damping behavior not accounted for in the design of the machine tool. Previous work with a milling process has also shown that the use of a microphone for measurements of this type is feasible in a laboratory setting, at low frequencies [10, 11].

Acoustic emissions from machining processes are attributable to the behavior of the material being processed and the parameters that define that process [12]. Acoustically emitted waves can be detected as elastic stress waves propagating from the deformation zone of a material undergoing machine processes [13]. Acoustically emitted signals from the deformation zones are detected in the form of either continuous emissions or discrete bursts. The shearing process emits a continuous signal that originates from the shearing zone. Discrete bursts occur upon chip separation of deformed material from the workpiece. The acoustic energy has been attributed to the following source mechanisms:

1. Primary deformation zone (shear zone)
2. Secondary deformation zone (tool-chip interface)
3. Tertiary zone (rubbing and friction between the tool flank and newly machined surface)
4. Chip breaking and entanglement
5. Tool degradation and fracture [13]

The primary deformation shear zone is the largest source of detectable acoustic vibrations, contributing up to 75% of expended emission energies [13]. These sources have been identified using a contacting sensor system.

Mechanisms for emissions have been refined in [14] and are given as [3]:

1. Plastic deformation during the cutting process in the workpiece
2. Plastic deformation in the chip
3. Frictional contact between the tool flank face and workpiece
4. Frictional contact between the tool rake face and the chip
5. Collisions between the chip and the cutting tool
6. Chip fracture
7. Tool fracture

These mechanisms were also identified using a contacting sensor in line with the cutting tool.

Machining hard metals has proven to produce acoustically emitted energies of up to two orders of magnitude greater than those of softer metals [15]. The unique deformation tendencies and chip structures for harder metals result from dislocation motion, twinning, inclusion fracture, decohesion, crack initiation, crack propagation, phase transformational attributes, and frictional components, as detailed in [15]. Hard metals exhibit increased levels of resistance to permanent deformation when subjected to applied load. The unique attributes of hard metal deformation are shown in Fig. 1. Experiments described in [15] proved correlation in agreement with the formation of saw-toothed chip geometries, common deformation tendencies to turning of hard metals, and an increased magnitude of signals emitted from the deformation zones.

Modes of tool wear, rake angle, undeformed chip thickness, and feed rate also affect the amount of elastic strain energy released that may be measured as transmitted acoustic energy. Tool wear occurs as a result of abrasive, chemical, adhesive, thermal, and mechanical conditions induced in the deformation zones. Differing types of tool wear dictate the manner in which a material deforms as it is being machined, subsequently increasing or decreasing the magnitude of released acoustical energy from the deformation zones. The primary types of tool wear include flank, crater, built-up edge, notch, plastic, thermal, and edge chipping wear. The frictional interface between the cutting edge and the material being machined changes with respect to the type and level of tool wear observed. Discerning the contributions of tool wear and material deformation elastic stress waves as acoustically emitted energy is discussed in [16].

Setting a tool's rake angle outside of the manufacturer's recommended working envelope has been proven to result in accelerated tool wear. The rake angle drives the contact area between the cutting edge and material being machined, yielding higher or lower main cutting forces applied at the deformation zone [17]. Saini and Park [13] confirmed that the described rake angle relationship and its effect on deforming material morphology is related to elevated acoustic emission events.

The undeformed chip thickness is equal to the depth at which the tool is cutting into the workpiece. As the tool's cutting edge increasingly penetrates the workpiece, a greater area of the tool induces deformation on the workpiece. With an increasing area of deformation, greater frictional and penetrative force is applied resulting in the release of elastic stress waves from the deformation zones. The undeformed chip thickness morphological tendencies are driven by the rate at which the tool penetrates the workpiece. The penetrating velocity of the cutting edge in relation to the rotating work for lathe turning is called the feed rate. Increasing or decreasing the feed rate affects the temperatures at the cutting edge interface. These phenomena were experimentally explored in [15]. It is important to note that most work done in this field has concentrated on energy methods concerned with characterization of time domain signals through integration rather than concentration on the frequency content of the emissions detected. Basic frequency domain behavior was discussed in [15], but no analytical or empirical model was postulated.

The frequency content of acoustic emissions was discussed in [18], with a frequency range from DC to 1 MHz evaluated. This work showed that the turning process produces ultrasonic emissions, with most energy emitted below 50 kHz. This work

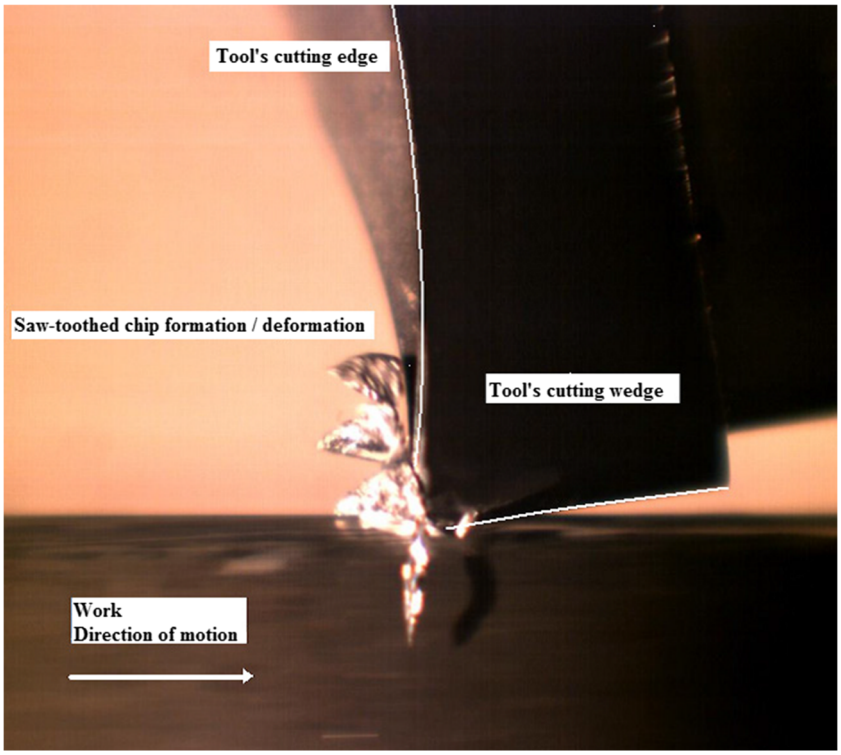


**Fig. 1** Orthogonal cutting test performed by one of the authors (Nelson), showing energy released through saw-toothed chip deformation

used a contacting sensor rather than a microphone for data acquisition. The authors comment on the effect of the structure of the machine tool and its possible effect on the bandwidth of the acquired signal.

Chip formation and material removal associated with the single-point turning process offers many potential acoustic sources for exploitation for machining process control or material identification purposes. This work uses a noncontacting sensor to characterize the acoustical emissions of four materials selected as machining surrogates for a strategic material, undergoing single-point turning, in order to establish proof of concept and to justify further study.

## 2 Experimental studies

### 2.1 Experimental setup overview

This work was conducted in a working machine shop environment located on a university campus. The turning operations that formed the basis of the work were performed on a manual lathe with fixed drive gear ratios. This machine tool was manufactured in 1946 by Monarch lathes and is shown in Fig. 2.

The acoustic measurements were gathered with measurement microphones placed as shown in Fig. 3. The placement of these sensors was established based on the expected frequency content of the signals to be measured and the associated attenuation of this frequency band by transmission through the atmosphere [19].

### 2.2 Machine tool details

This study used a manual lathe for performing the turning work used as the measured phenomenon. This machine tool has a 305-mm (12 in.) diameter chuck and a 368-mm (14.5 in.) swing and measures 762 mm (30 in.) between centers. The operation measured was single-point outer diameter turning of solid cylindrical billets of select materials that were of interest to the sponsor of the research. The machine tool has a spindle drive with fixed gear ratios. Data were gathered using input excitation at 58, 98, 158, and 319 rpm, which were presets for the machine tool. These machining speeds were dictated by the sponsor of the research. While these cutting speeds are lower than one would expect in most production

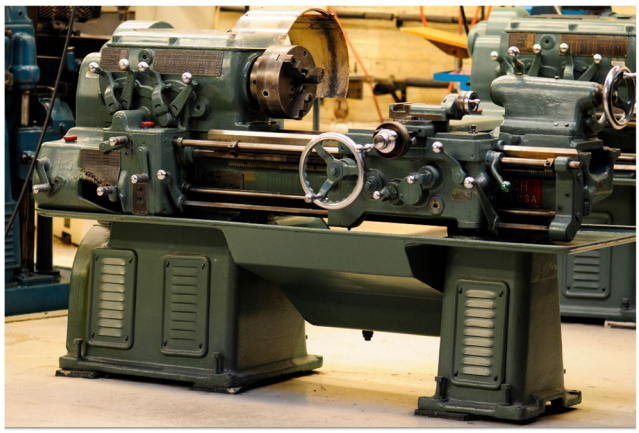

**Fig. 2** Manual lathe used in generating acoustic measurements

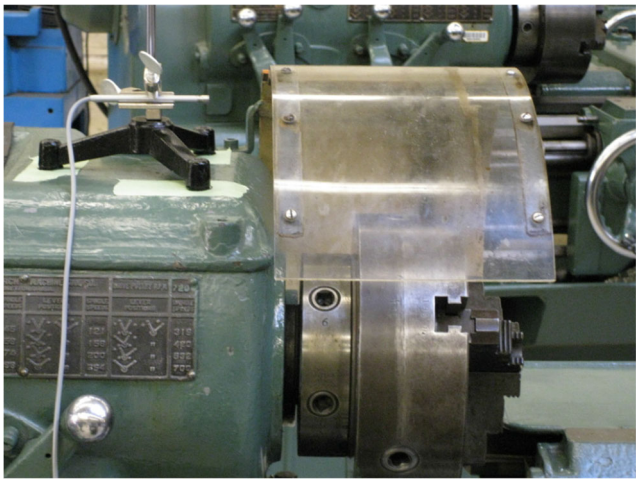

**Fig. 3** Microphone placement for data acquisition

operations, they are appropriate for the materials being processed in this work. See [20] for exploration of this phenomenon at lower cutting velocities. Equation (1) is used to convert these spindle speeds to excitation frequencies for the mechanical system:

$$\omega = \frac{2\pi n}{60}, \tag{1}$$

where $\omega$ is the circular frequency in radians/second, and $n$ is the spindle speed in revolutions/minute. Equation (2) is used to convert values to linear frequency:

$$f = \frac{\omega}{2\pi}, \tag{2}$$

where f is the linear frequency in Hertz. These transformations yield input excitation frequencies of 1, 1.6, 2.6, and 5.3 Hz, respectively.

### 2.3 Cutting tool and cutting tool holder

The turning operation was conducted using a Kennametal MVJNR-203D outside diameter right-hand tool holder, fitted with replaceable cutting inserts. The cutting tool inserts used were Kennametal ANSI VNMS 332 (ISO VNMS 160408) K68 and ANSI VNMS 332 (ISO VNMS 160408) KC730 carbide metal cutting inserts. These cutting inserts are identical in geometry [21].

The difference between the two cutting tool inserts used is the application of a titanium nitride (TiN) coating to the KC730 grade inserts, which is recommended by the cutting tool manufacturer when processing certain materials. These inserts were rotated or replaced for every cutting operation measurement in order to present a new edge to the workpiece for each data set. This step mitigated observed variability in the processes due to cutting tool wear. Prior to commencing a turning pass, the tool was placed in proximity to the work using a shim, with the operator removing backlash in the turning feed mechanism. Once the cutting tool was fully engaged, noise measurement data were acquired.

### 2.4 Acoustic measurement equipment

Acoustic measurements were obtained using a Brüel & Kjaer type 4939 free-field microphone, held in a rigid stand. The microphone signal was processed using a Brüel & Kjaer NEXUS type 2690 two-channel conditioning amplifier. The free-field microphone was chosen based on the assumption that the source of the measured signal would be known and that a reverberant field would not be present in the space where the experiment would be conducted. A small form factor was also chosen to minimize the effect the microphone may have on the measured sound field. The microphone sensitivity is given as 4.2 mV/Pa and the microphone/preamplifier combined sensitivity is 4.09 mV/Pa [22]. This microphone/preamplifier combination was selected to accommodate the anticipated frequency range of interest for the experiment.

The analog output from the amplifier was digitized using hardware set to sample the signal at 200 kHz. These data were imported into commercially available data acquisition software for recording. Data samples were collected for a minimum of 30 s (six million samples) for each measurement condition. Data collection was initiated after the machining process had reached steady state (i.e., full cutting tool engagement) to exclude any transient behavior from the measurements.

### 2.5 Experimental design

This work was applied to four materials of interest. The materials used are shown in Table 1. Material samples were inspected using a portable X-ray fluorescence (XRF) device and verified to be within specification [23].

The measurements made in this study varied using three basic parameters associated with single-point turning operations: depth of cut, spindle speed, and cutting tool feed rate. The ranges of these varying parameters were suited to the processing of the selected materials. Experimental study materials along with process parameter settings are shown in Table 2. Cutting velocity was obtained using the spindle fixed gear relationships along with the diameter of the workpiece at the time the experimental cutting operation was performed, using Eq. (3):

$$v = \frac{\omega \varnothing}{2}, \tag{3}$$

where $v$ is the cutting velocity in millimeters/second, and $\varnothing$ is the diameter of the workpiece in millimeters, with angular velocity, $\omega$, expressed in radians/second.

**Table 1** Experimental materials

| Unified numbering system identifier | Common name | Modulus of elasticity (GPa) | Ultimate strength (MPa) | Hardness (Rockwell B) | Poisson's ratio | Density ($kg/m^3$) |
|---|---|---|---|---|---|---|
| UNS A96061 | Aluminum 6061 | 68.9 | 310 | 60 | 0.33 | 2700 |
| UNS T11342 | M42 high speed tool steel | 207 | 2560 | 100 (annealed) | 0.285 | 8100 |
| UNS S24000 | Nitronic 33 stainless steel | 193 | 793 | 100 (annealed) | 0.305 | 7775 |
| UNS R05255 | Tantalum tungsten alloy (Ta2.5W) | 195 | 345 | 70 | 0.35 | 16,660 |

### 2.6 Experimental environment

The machine tool used in this study was situated in a machine shop, among and around other machine tools, with room finishes typical of an industrial work space, concrete floors, hard walls, and ceiling open to building structure.

The measurement microphone was placed in close proximity to the tool/workpiece interface, but at a sufficient distance to avoid contact with chips or cutting fluid [19]. The distance between the microphone and the point of cutting tool initial contact was measured to be approximately 381 mm (15 in.). This distance was chosen to minimize attenuation of ultrasonic frequencies in the emitted signal while allowing room for the machine operator to access the equipment without disturbing the microphone placement.

In order to eliminate the contribution of ambient noise and vibration in the shop space, and to account for noise intrinsic to machine tool spindle rotation, background measurements were made prior to collecting data for each experimental parameter set. The noise data represent the ambient noise, along with noise attributable to machine tool spindle rotation without having the cutting tool in contact with the workpiece.

**Table 2** Experimental variation of parameters

| Trial number | Material | Cutting tool grade[a] | Depth of cut (mm) | Tool feed rate (μm/revolution) | Cutting velocity (mm/s) | Sample diameter (mm) |
|---|---|---|---|---|---|---|
| 1 | AL 6061 | K68 | ***0.51*** | ***76.2*** | ***1057*** | ***128*** |
| 2 | AL 6061 | K68 | 1.02 | 76.2 | 1052 | 127 |
| 3 | AL 6061 | K68 | *0.51* | *76.2* | *498* | *97* |
| 4 | AL 6061 | K68 | *0.51* | *76.2* | *1615* | *97* |
| 5 | AL 6061 | K68 | **0.51** | **152.4** | **1006** | **122** |
| 6 | AL 6061 | K68 | **0.51** | **228.6** | **1001** | **121** |
| 7 | M42 tool steel | KC370 | ***0.51*** | ***76.2*** | ***1077*** | ***130*** |
| 8 | M42 tool steel | KC370 | 1.02 | 76.2 | 1067 | 129 |
| 9 | M42 tool steel | KC370 | *0.51* | *76.2* | *523* | *102* |
| 10 | M42 tool steel | KC370 | *0.51* | *76.2* | *1712* | *102* |
| 11 | M42 tool steel | KC370 | **0.51** | **152.4** | **1041** | **126** |
| 12 | M42 tool steel | KC370 | **0.51** | **228.6** | **1036** | **125** |
| 13 | N33 stainless | K68 | **0.51** | **76.2** | **1062** | **207** |
| 14 | N33 stainless | K68 | 1.02 | 76.2 | 1057 | 206 |
| 15 | N33 stainless | K68 | *0.51* | *76.2* | *620* | *204* |
| 16 | N33 stainless | K68 | *0.51* | *76.2* | *1681* | *203* |
| 17 | N33 stainless | K68 | **0.51** | **152.4** | **1041** | **203** |
| 18 | N33 stainless | K68 | **0.51** | **228.6** | **1036** | **202** |
| 19 | Ta2.5W | KC370 | ***0.51*** | ***76.2*** | ***1341*** | ***162*** |
| 20 | Ta2.5W | KC370 | 1.02 | 76.2 | 1336 | 161 |
| 21 | Ta2.5W | KC370 | *0.51* | *76.2* | *635* | *124* |
| 22 | Ta2.5W | KC370 | *0.51* | *76.2* | *2047* | *123* |
| 23 | Ta2.5W | KC370 | **0.51** | **152.4** | **1275** | **154** |
| 24 | Ta2.5W | KC370 | **0.51** | **228.6** | **1275** | **154** |

Italicized and bolded data sets form groups for comparison (see Section 4)

[a] All cutting tools used were of VNMS 332 type

These background noise measurements were examined and averaged for use as a datum with the recorded experimental measurements. The average background noise signature is shown in Fig. 4. Note that the signal is voltage displayed as a function of frequency on a logarithmic scale. This represents the digitized output of the sensor in raw form.

Acoustical noise measurements are typically given in decibels with a reference pressure that is nominally equivalent to the threshold of normal human hearing (dB re 20 μPa) [24]. Since the frequency band of interest here spans from 10 to 100 kHz (the "normal" range of human hearing is 20–20 kHz) [24]), this convention is of limited value, other than to give an indication of the audible background noise level that was present during experimental data collection. Use of the decibel unit is tied to the sensitivity of the human ear and to the acoustics of workplace noise. For reference, $10^{-1}$ V converts to 121.8 dB re 20 μPa, with the sound pressure level dropping 20 dB per decade as the voltage decreases (e.g., $10^{-2}$ V = 101.8 dB). Since the raw measurements are of interest in this work, the data will be displayed in that form, rather than using the conversion to the decibel scale. It should also be noted that although data have been acquired for frequencies below 125 Hz, these data are regarded as unreliable, per normal measurement practice. Room dimensions of less than 3 m (usually the floor to ceiling measurement) do not support accurate measurement of low-frequency sound [25].

### 2.7 Analysis of data

Data sets in the time domain were gathered using the experimental apparatus referenced. These data were then transformed into the frequency domain using commercially available software. The software utilized a 4096 sample Hann window function [26], with 50% overlap to generate the frequency response data shown. A typical data set is shown in Fig. 5.

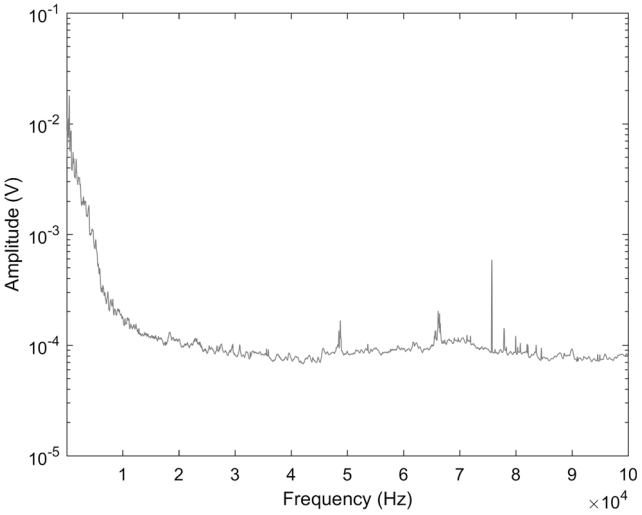


**Fig. 4** Ambient noise in the experimental space

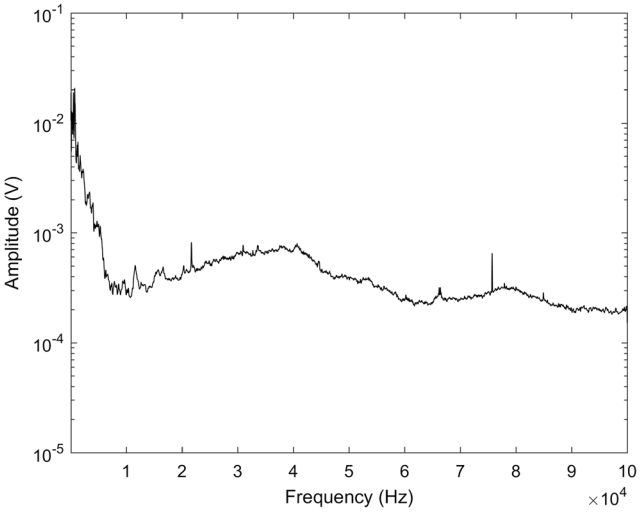


**Fig. 5** Acoustic data for turning aluminum 6061 at 1001 mm/s with 0.51 mm depth of cut and a feed rate of 152.4 μm per revolution

## 3 Experimental results and discussion

### 3.1 Background noise, audible region

A close examination of Fig. 4 shows that the background noise in the shop is of significant amplitude in the audible range. A significant peak is present at 550 Hz. The general character of the noise demonstrates an amplitude roll off at around 20 dB per decade but remains of significant amplitude below 10 kHz. Note the high levels of noise present in the frequency range bounding the input excitation from spindle rotation (1–10 Hz).

### 3.2 Background noise, ultrasonic region

In Fig. 4, significant peaks are observed around 48.8, 66.2, and 75.7 kHz. The general character of the noise in the ultrasonic region is a flat response, other than the peaks noted.

### 3.3 General observations

The sampling rate of the digitizing hardware set the Nyquist frequency of the measurement at 100 kHz [27]. This frequency range was selected based on preliminary measurements of background noise in the shop environment where testing was to be accomplished and the assumption that the structures studied in this work were of sufficient stiffness that measurable ultrasonic energy would be present, and that the turning process for the materials of interest in this study would track the behavior shown in reference [15].

Sound pressure levels attributable to machining operations are shown to be detectable using the instrumentation chosen for this study. Sound pressure levels that are differentiated from the ambient noise in the machine shop environment were observable in every measurement case. Figure 6 is a typical

example of the comparison between the background noise present and the measured noise attributable to turning operations.

The excess sound attributable to machining operations occurs mainly in the ultrasonic frequency range. Figure 4 illustrates the distribution of the emitted acoustic energy, with most of the emissions coming in the ultrasonic ($f > 2 \times 10^4$ Hz) frequency range. It is shown in reference [15] and in Section 4 that chip formation in the turning process, the workpiece being turned, and the cutting tool holder are likely sources of ultrasonic emissions.

Frequency content was distinct for each individual type of material tested at high cutting tool feed rates. Nitronic 33 stainless steel radiated energy at levels above background beginning at a much lower frequency (~3 kHz), as compared to the other materials evaluated (~6 kHz) and as shown in Fig. 7.

Identification of signal characteristics is limited to occurrence, amplitude, and frequency of significant signal peaks read from the Fourier transform (FFT) results shown. More complex signal analyses, such as coherence estimation, cross correlation function generation, cepstrum analysis, or wavelet analysis, are dependent on the strategy for signal detection and are left for future work.

### 3.4 Material specific observations

#### *3.4.1 Aluminum alloy 6061*

For aluminum alloy 6061, an increase in spindle speed resulted in increased radiation of energy in the region between 6.1 and 66 kHz, as shown in Fig. 8.

The noise generated was similar at the two lower values of the cutting speed studied. When the cutting velocity was increased to 1615 mm/s, the frequency range of increased radiated sound expanded to between 8 and 100 kHz. Increasing

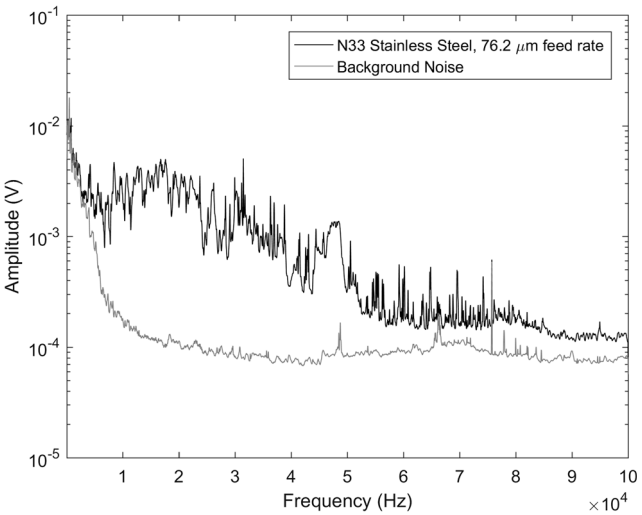


**Fig. 6** Comparison between a turning operation and background noise

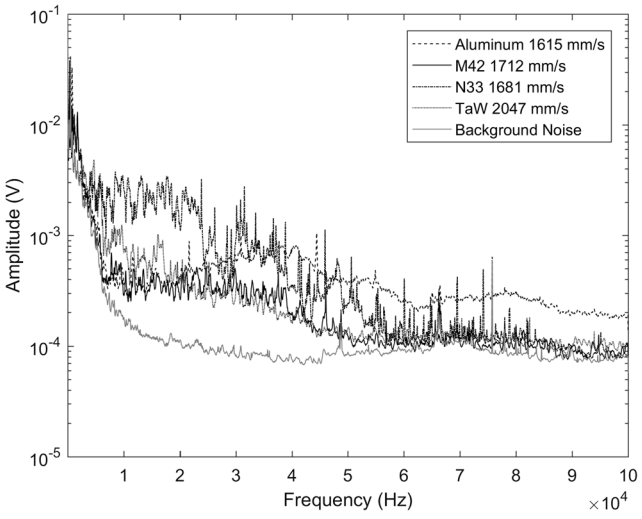


**Fig. 7** Detectable radiation onset frequency for Nitronic 33 stainless steel at high cutting speed

the cutting tool feed rate produced similar results, with sound power levels increasing with increasing feed rate, as shown in Fig. 9.

Increasing spindle speed and feed rate produced no persistent recurring peaks. Increasing depth of cut produced similar behavior with respect to radiated frequency range. Figure 10 shows that several prominent peaks are present.

#### *3.4.2 Nitronic 33 stainless steel*

Increase in spindle speed for the Nitronic 33 stainless steel material resulted in increased radiation of energy in the region between 3.2 and 70 kHz, as shown in Fig. 11. Low spindle speed (620 mm/s) produced a detectable increase in sound pressure level above ambient conditions.

Higher spindle speeds produced higher sound pressure levels, which were difficult to differentiate based on cutting

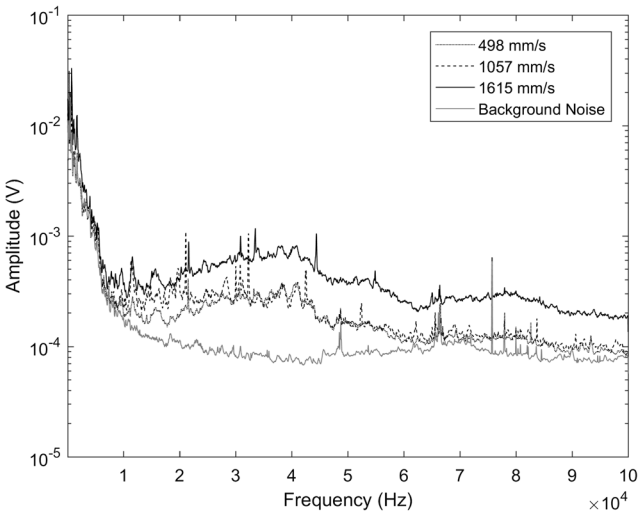


**Fig. 8** Acoustic emissions from aluminum 6061 with varying cutting speeds

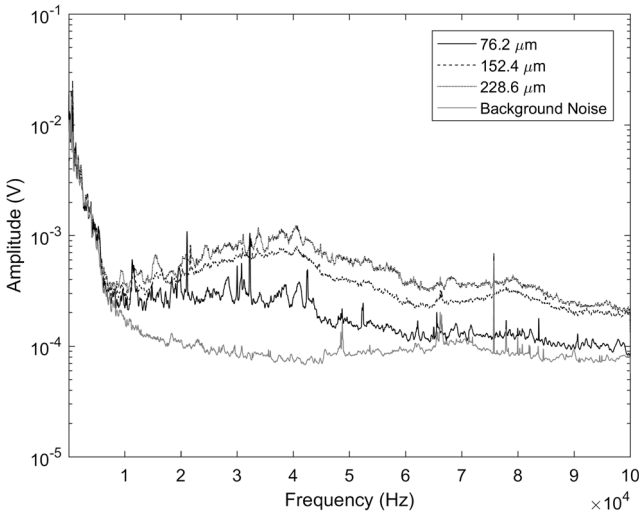


**Fig. 9** Acoustic emissions from aluminum 6061 with varying cutting tool feed rates

velocity. Increasing feed rate did not produce noise signatures that were distinguishable. The same behavior was demonstrated when depth of cut was varied.

### *3.4.3 M42 tool steel*

The M42 tool steel was processed at increased spindle speed when compared to Nitronic 33 stainless steel, which resulted in increased radiation of energy in the region between 6.3 and 65 kHz, as shown in Fig. 12.

Noise signatures for different cutting speeds were indistinguishable when processing this material. Increasing cutting tool feed rate did produce distinguishable noise signatures between 28 and 65 kHz. Increasing depth of cut did not produce differentiable noise signatures.

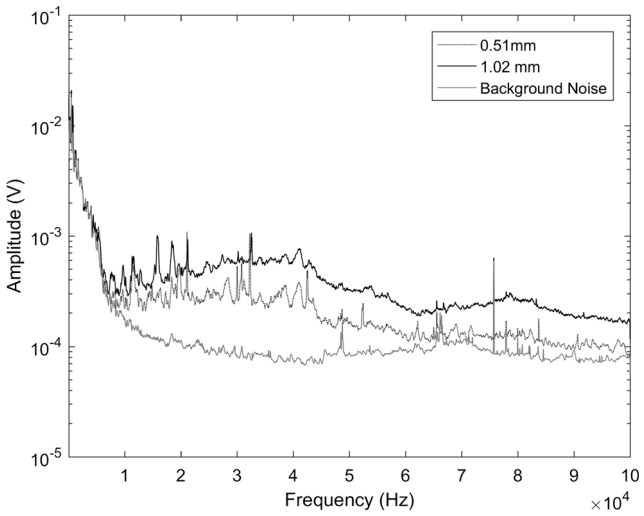


**Fig. 10** Acoustic emissions from aluminum 6061 with varying depth of cut

### *3.4.4 Tantalum tungsten (Ta2.5W) alloy*

For the tantalum tungsten (Ta2.5W) alloy, increase in spindle speed resulted in increased radiation of energy in the region between 3.6 and 65 kHz, as shown in Fig. 13.

Variation of the other experimental process parameters produced no discernable changes in noise signature.

## 3.5 Operation-specific observations

### *3.5.1 Cutting speed*

Low spindle speed cutting operations did not produce noise signatures that were readily discernable with the experimental material used in this study. Medium spindle speed yielded a noise signature for Nitronic 33 stainless steel that was easily differentiable from the noise produced by the other materials under study, as shown in Fig. 14.

Operation at high spindle speeds produced a distinct signature for aluminum 6061 above 25 kHz, while the other two materials remained undistinguishable, as shown in Fig. 15.

### *3.5.2 Cutting tool feed*

At the lowest feed rate (76.2 μm per revolution), Nitronic 33 produced a discernable noise signature over a large frequency range. Aluminum 6061 produced a noise signature identifiable over a narrow band of frequencies, between 35 and 60 kHz, as seen in Fig. 16.

As feed rate increases, the noise signatures of the individual materials become easily distinguishable, as shown in Fig. 17.

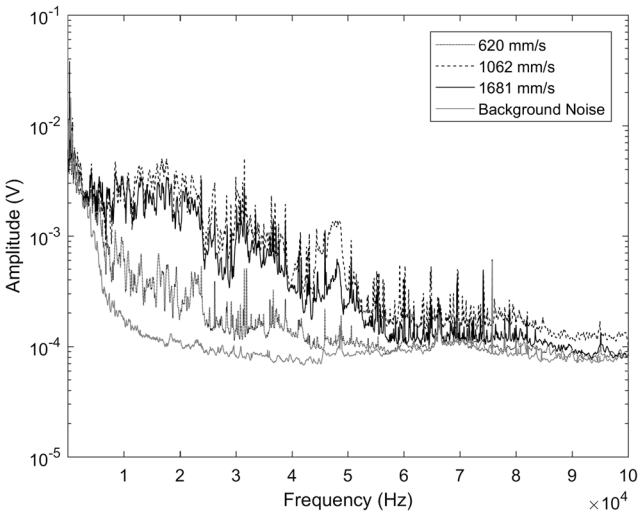


**Fig. 11** Acoustic emissions from Nitronic 33 stainless steel with varying cutting velocities

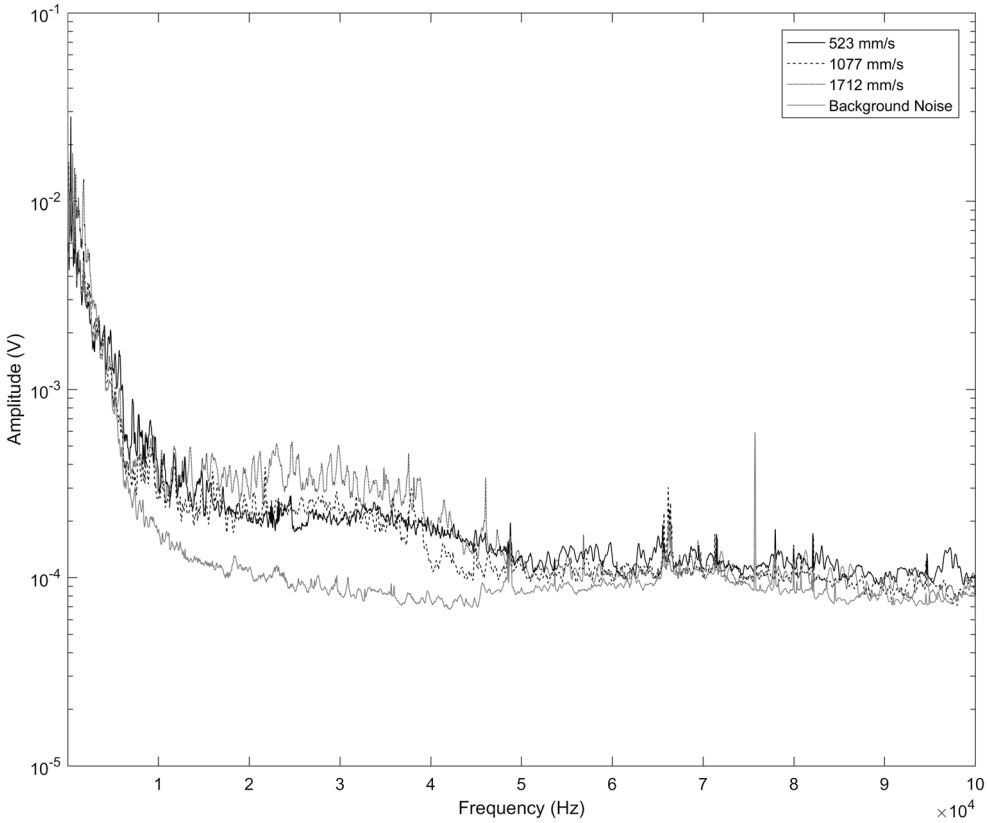


**Fig. 12** Acoustic emissions from M42 tool steel with varying cutting velocities

*3.5.3 Depth of cut*

Noise signatures for a cut depth of 0.51 mm were indistinguishable, with the exception of Nitronic 33 stainless steel, as shown in Fig. 18.

Increasing the depth of cut to 1.02 mm yielded discernable noise signatures for Nitronic 33 stainless steel and aluminum 6061. Measurements for M42 tool steel and tantalum tungsten produced indistinguishable noise signatures, as seen in Fig. 19.

## 4 Discussion and conclusions

### 4.1 Relationship between basic material properties and acoustic emissions

Measurements conducted in this study show that the acoustic energy emitted and detected is not a function of the basic material properties shown in Table 1. While N33 and M42 steels have the same nominal annealed hardness values, their

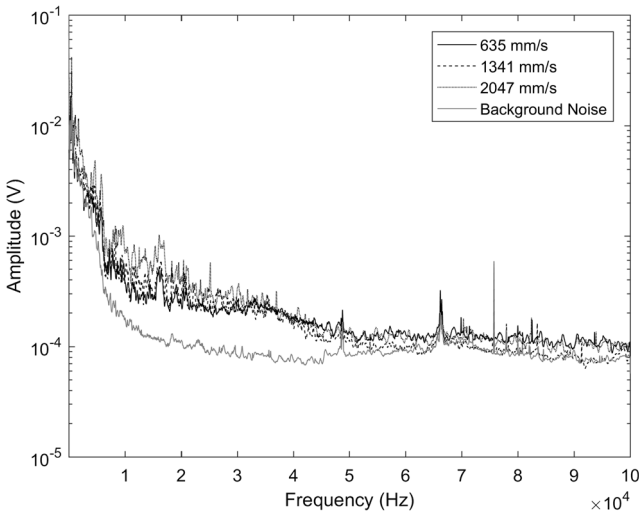


**Fig. 13** Acoustic emissions from Ta2.5W alloy with varying cutting velocities

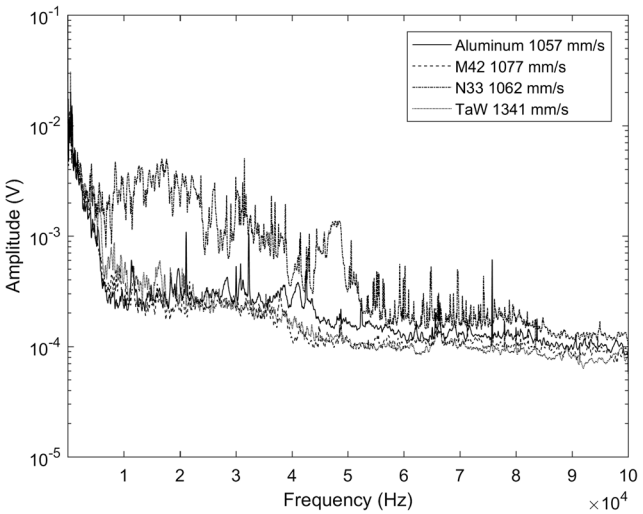


**Fig. 14** Comparison of experimental material acoustic emissions at medium cutting speed

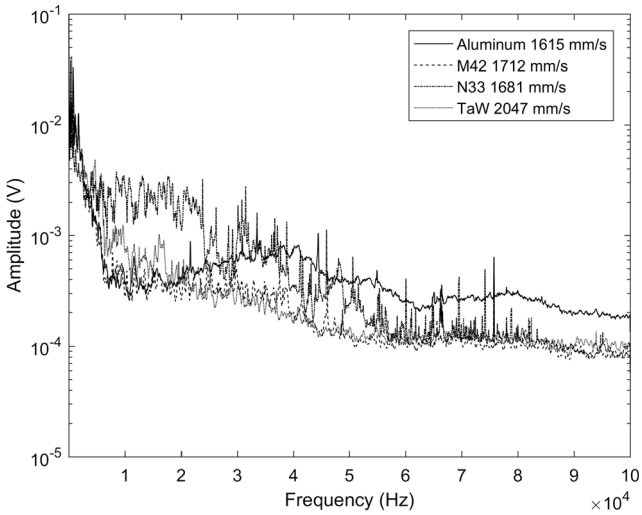


**Fig. 15** Comparison of experimental material acoustic emissions at high cutting speed

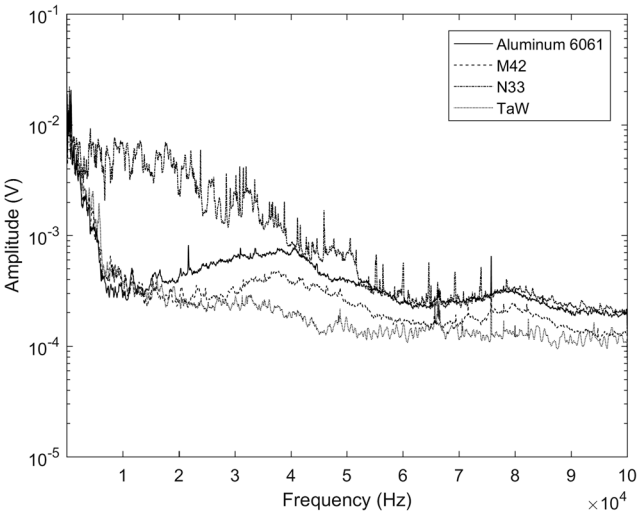


**Fig. 17** Comparison of experimental material acoustic emissions at high cutting tool feed rate (228.6 μm per revolution)

acoustic signatures vary greatly, and counterintuitively, in inverse proportion to their ultimate strengths. This is further evidence to support inadequacy of the single shear plane model of chip formation discussed in [28], assuming that shear strength is proportional to ultimate strength for the materials tested.

### 4.2 Macroscopic acoustic emission mechanism analysis

Two possible mechanisms for acoustic emissions that can be analytically evaluated are as follows:

1. Flexure of the workpiece
2. Flexure of the tool holder assembly

Each of these structures is inherently stiff with respect to displacement due to processing, which is a basic assumption used to design machine tool processes. The workpieces in this study were restricted to cantilevered lengths of 102 mm (4 in.) maximum. The tool holder was secured in the tool post assembly, with the cantilever portion of the assembly limited to the triangular section shown in Fig. 20.

These structures both fall within the regime of structures usually modeled using Timoshenko beam theory rather than Euler-Bernoulli beam theory.

The boundary conditions for the two structures proposed as radiating mechanisms can be modeled as fixed on one end and free on the other end. The input excitation is attributable to the circular frequency of the rotation of the workpiece added to the high-frequency excitation attributable to the stick-slip of

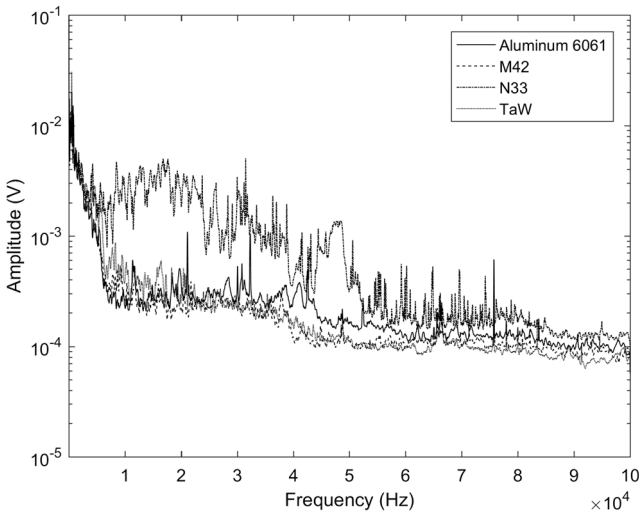


**Fig. 16** Comparison of experimental material acoustic emissions at low cutting tool feed rate (76.2 μm per revolution)

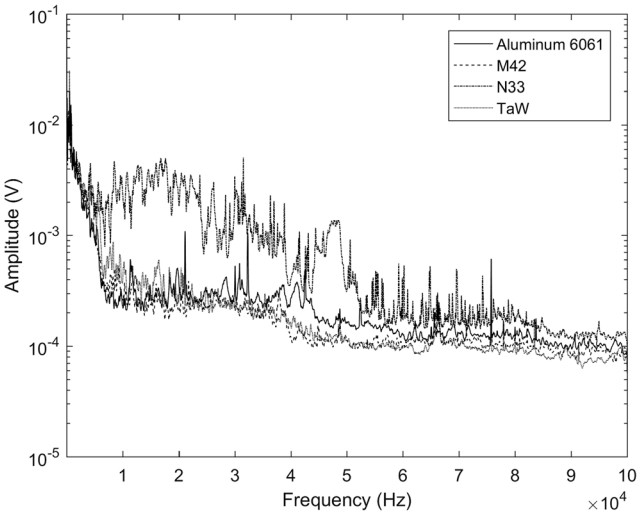


**Fig. 18** Comparison of experimental material acoustic emissions at 0.51 mm cutting depth

the cutting tool and the plastic deformation of the chip as it is separated from the workpiece [15].

Timoshenko beam theory preserves the shear displacement and the rotary displacement omitted in Euler-Bernoulli beam theory, producing a more accurate estimation of vibration behavior for structures that do not meet the criteria of a "long, slender" structure assumed by that development [29].

Using the Timoshenko theory, the fundamental flexure frequency of the workpiece would be found using Eqs. (4), (5), (6), and (7) [30]:

$$s^2 = \frac{\left(\gamma^2 b^2 + a^2\right)\left(a^2\gamma^2 + b^2\right)}{\left(a^2 - b^2\right)\left(1 + \gamma^2\right)} \tag{4}$$

$$s^2 = \frac{\left(-\gamma^2 \tilde{b}^2 + a^2\right)\left(a^2\gamma^2 - \tilde{b}^2\right)}{\left(a^2 + \tilde{b}^2\right)\left(1 + \gamma^2\right)} \tag{5}$$

$$\left(a^2 - b^2\right)\sin a \sinh b - ab\frac{\left(a^4 + a^4\gamma^4 + 4\gamma^2 a^2 b^2 + b^4\gamma^4 + b^4\right)}{\left(b^2 + \gamma^2 a^2\right)\left(a^2 + \gamma^2 b^2\right)} \cos a \cosh b - 2ab = 0 \tag{6}$$

$$\left(a^2 - \tilde{b}^2\right)\sin a \sinh \tilde{b} - a\tilde{b}\frac{\left(a^4 + a^4\gamma^4 + 4\gamma^2 a^2 \tilde{b}^2 + \tilde{b}^4\gamma^4 + \tilde{b}^4\right)}{\left(\tilde{b}^2 + \gamma^2 a^2\right)\left(a^2 + \gamma^2 \tilde{b}^2\right)} \cos a \cosh \tilde{b} - 2a\tilde{b} = 0 \tag{7}$$

where $s$ is the slenderness ratio, with $a$ and $b$ being dimensionless wavenumber components. The wavenumber components are related to the vibration frequency by Eq. (8) [30]:

$$\omega = \frac{1}{\gamma}\sqrt{\frac{E\left(a^2 - b^2\right)}{\rho L^2}} \tag{8}$$

where $E$ is the Young's modulus, $\rho$ is the mass density, and $L$ is the length of the cantilever beam. $\omega$ is produced in radians/second.

$\gamma$ is given in Eq. (9) as [30]

$$\gamma = \sqrt{\frac{2(1+\upsilon)}{k'}} \tag{9}$$

where $\nu$ is Poisson's ratio and $k'$ is a shear factor determined by the cross section shape of the beam. For this work, we use Eq. (10) for a circular cross section (the workpiece) [31]:

$$k' = \frac{6(1+\nu)}{7+6\nu} \tag{10}$$

and Eq. (11) for a rectangular cross section (the tool holder assembly) [31]:

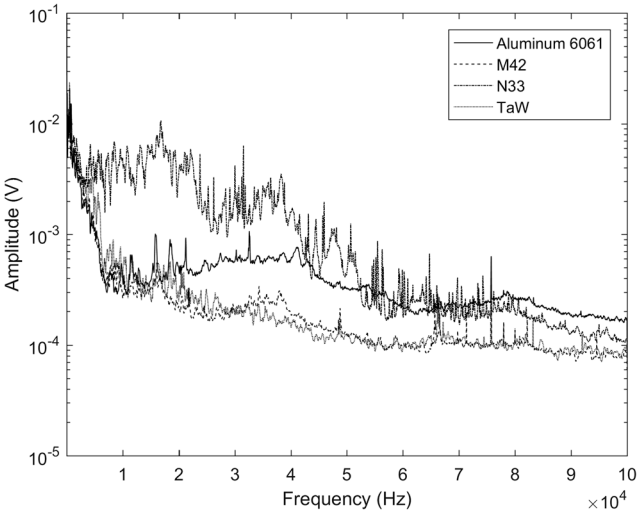


**Fig. 19** Comparison of experimental material acoustic emissions at 1.02 mm cutting depth

$$k' = \frac{10(1+\nu)}{12+11\nu} \tag{11}$$

Timoshenko beams vibrate in two frequency regimes, separated by a cutoff frequency defined by a critical value of the first wavenumber component, $a$, shown in Eq. (12) [30]. At this value, the wavenumber component $b$ vanishes to zero.

$$a_c = s\sqrt{\frac{1}{\gamma^2} + 1} \tag{12}$$

When the value of $a$ is below the critical value, Eqs. (4) and (6) are solved simultaneously to determine the values of $a$ and $b$. These wavenumber components are then used to determine frequency of flexural vibration in the structure. When $a$ is larger than the value of $a_c$, then Eqs. (5) and (7) are used to find $a$ and $\tilde{b}$. Then, $a$ and $\tilde{b}$ are used to find the frequency of flexural vibration.

Table 3 shows the frequencies of vibration of the first four modes of each of the structures of interest in this work, the four material workpieces, and the tool holder assembly.

The tool holder assembly is handled here using the beam relationship for a constant cross section. Since the cross

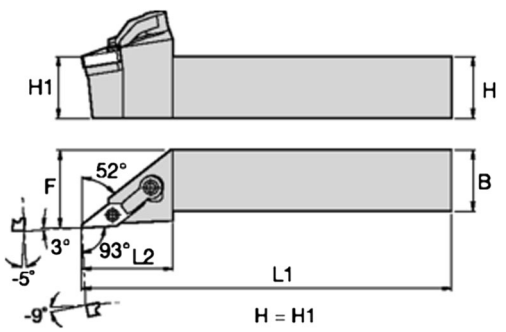


**Fig. 20** Cantilever portion detail of the tool holder assembly [21]

section is not of constant shape, an average for second moment of area and for the shear factor, $k'$, have been used in the expression for determining vibration frequency, since the variation in cross section takes place in the horizontal dimension, which is linear in the expression for second moment of area for a rectangular cross section. The expression for shear factor, given in Eq. (11) for a rectangular cross section, is also linear in this dimension.

Review of the data shown in Table 3 illustrates that the geometry of the bodies identified as potential radiators of sound do contribute to the acoustic energy in the frequency range of interest for this work. Modes 2, 3, and 4 of the tool holder, as well as the 4th mode for aluminum 6061, M42 tool steel, and Nitronic 33 stainless steel workpiece, fall into the ultrasonic range of frequencies. Note that the three workpieces produce similar frequency content, indicating that this phenomenon may not be a viable mechanism for differentiation of material behavior. The high mass density of the tungsten tantalum alloy causes that particular structure to radiate below ultrasonic frequency, following the mass law relationship,

$$\omega \propto \sqrt{\frac{k}{m}} \tag{13}$$

with $k$ being the general stiffness of the structure and $m$ being the structure mass.

The individual predicted peaks associated with the tool holder given in Table 3 can be seen conceptually in Figs. 6, 8, and 13, with peaks near the designated frequencies that do not appear in the background noise signal. Even with these mechanisms identified, the broadband nature of the acoustic signal again points to the generation mechanisms discussed in [14, 15]. The mechanisms quantified in Table 3 would need to be augmented with a complete analysis of the machine tool for characterization of frequency contribution by specific features of the system, a partial example of which is shown in [32].

### 4.3 Microscopic acoustic emission mechanism discussion

The other obvious possibility is that the chip resulting from the turning operation is contributing to the acoustic emission measured in this work. Chip width is a controlled parameter in turning operations, as is chip thickness. Since the deformation and failure in the crystal lattice is happening in the direction of the chip thickness, this dimension is a natural choice as a radiation mechanism. The reader is directed to [14] for a discussion of mechanisms for generation of acoustic energy in the ultrasonic range, albeit at cutting speeds greater than those considered in this work. Special attention is required to the discussion of the limits of the contact sensing equipment used in this study, which was one consideration for selection of the noncontacting sensor used by the authors.

**Table 3** Flexural vibration frequencies for structures of interest

| Structure | Tool holder | Al 6061 | M42 tool steel | N33 stainless steel | Tantalum tungsten alloy |
|---|---|---|---|---|---|
| Mode | Vibration frequency, kHz | | | | |
| 1 | 10.4 | 4.3 | 4.3 | 4.7 | 3.2 |
| 2 | 28.6 | 12.1 | 12.1 | 12 | 8.1 |
| 3 | 46.6 | 20.1 | 20 | 18.3 | 12.8 |
| 4 | 64.2 | 26.8 | 26.9 | 26.8 | 18.4 |

### 4.4 Use of acoustic emissions as input for machine control algorithms

The use of this method as a control input is dependent on the behavior of the acoustic signatures as cutting speed varies and as cutting tool feed varies. Normal processing would see depth of cut set as a constant, with speed and feed varied to push the process to the stability limit where chatter would result. The formula for chip width used in the generation of stability lobe diagrams is given as [33]:

$$b = \frac{-1}{2k_s G_R}, \tag{14}$$

where $b$ is the chip width, $k_s$ is the stiffness of the cutting tool, and $G_R$ is given by [33]:

$$G_R = Re\left(\frac{x}{F}\right) = \frac{1-r^2}{k\left[(1-r^2)^2 + (2\zeta r)^2\right]} \tag{15}$$

where $x$ is the displacement of the cutting tool, $F$ is the cutting force, $k$ is the stiffness of the workpiece, $\zeta$ is the damping ratio, and $r$ is the frequency ratio, given by [33]:

$$r = \frac{f_{Spindle}}{f_{Natural}} \tag{16}$$

This leads to the spindle speed as the parameter of choice for variation, since classical stability theory holds that chip width and forcing frequency determine stability, independent of chip thickness.

Based on data gathered in this work, the control parameter selection would have to be based on the type of material to be processed, since neither cutting speed nor cutting tool feed rate was universally shown to provide a differentiable model. While this work did not study geometric effects attributable to the workpiece, such as hollow tubing compared to solid bar stock, vibration modes of the workpiece may interfere with, or mask, behaviors shown here.

Control methodologies using inline sensors have been published, see for example [34]. Reference [35] demonstrated that amplitude-based monitoring of machine processes using a

microphone is possible, even with the restriction of the sound monitoring to frequencies below 25 kHz. The method is at best indirect, however, and would need to be augmented for use as a true control system input.

It is interesting to note that the work done in [36, 37] could conceivably be adapted to the ultrasonic frequency range, given advances in analog to digital conversion sampling rate and computer processor speeds since the original publication of this work. These methods were accomplished using a microphone as a sensor.

### 4.5 Conclusion and future work

This study has shown that monitoring of machine tool vibration is feasible using a noncontact transducer with the caveat that the transducer and digitizing interface operate in the ultrasonic frequency band. Background noise in an industrial space is shown to be dominant in the audible region, especially with the low-frequency excitation of the workpiece inherent in single-point turning. This level of background noise masks the primary input/output behavior that would normally be leveraged in controlling the process [38]. Additional signal processing would be required to identify materials, since simple FFT/spectrum analysis was unable, in some instances, of distinguishing between materials or between process parameter states. Coherence estimation, cross correlation function generation, cepstrum analysis, and wavelet analysis are all candidate strategies for material or process-specific signal detection and differentiation. This area is left for future study.

**Compliance with ethical standards** This study did not involve human subjects, and therefore, no institutional review board approval was necessary.

**Conflict of interest** The authors declare that they have no conflicts of interest.

**Funding** There was no funding for this study.

## References

1. Astakhov V (2006) Generalized model of chip formation, in Tribology of metal cutting 2006. Elsevier Ltd., London
2. Eynian M, Altintas Y (2009) Chatter stability of general turning operations with process damping, J Manuf Sci Eng 131(4)
3. Siddhpura M, Paurobally R (2012) A review of chatter vibration research in turning. Int J Mach Tools Manuf 61:27–47
4. Merritt H (1965) Theory of self-excited machine tool chatter. ASME J Eng Ind 87:447–454
5. Yilmaz A, AL-Regib E, Ni J (2002) Machine tool chatter suppression by multi-level random spindle speed variation, J Manuf Sc Eng 124
6. Filippov A, Nikonov A, Rubtsov V, Dmitriev A, Tarasov S (2017) Vibration and acoustic emission monitoring the stability of peakless tool turning: experiment and modeling. Journal of Materials Processing Technology 246:224–234
7. Albertelli P, Musletti S, Leonesio M, Bianchi G, Monno M (2012) Spindle speed variation in turning: technological effectiveness and applicability to real industrial cases. Int J Adv Manuf Technol 62: 59–67
8. Li D, Mathew J (1990) Tool wear and failure monitoring techniques for turning—a review. Int J Mach Tools Manuf 30(4):579–598
9. Frumusanu G, Constantin I, Marinescu V, Epureanu A (2013) Development of a stability intelligent control system for turning. Int J Adv Manuf Technol 64:643–657
10. Delio T, Tlusty J, Smith S (1992) Use of audio signals for chatter detection and control. J Eng Ind 114
11. Choudhury S, Goudimenko N, Kudinov V (1997) On-line control of machine tool vibration in turning. Int J Mach Tools Manuf 37: 801–811
12. Dornfeld D, Pan C (1985) A study of continuous/discontinuous chip formation using acoustic emission. J Appl Metalwork 4(1)
13. Saini D, Park Y (1996) A quantitative model of acoustic emissions in orthogonal cutting operations. J Mater Process Technol 58:343–350
14. Liang S, Dornfeld D (1989) Tool wear detection using time series analysis of acoustic emission. J Eng Ind Trans ASME 111:199–205
15. Byrne J, Barry G (2001) Study on the acoustic emission in machining hardened steels part 1: acoustic emission during saw-tooth chip formation. J Eng Manuf 215:1549–1559
16. Chiou R, Liang S (2000) Analysis of acoustic emission in chatter vibartion with toll wear effect in turning. Int J Mach Tools Manuf 40:927–941
17. Günay M, Aslan E, Korkut I, Şeker U (2004) Investigation of the effect of rake angle on main cutting force. Int J Mach Tools Manuf 44:953–959
18. Grabec I, Leskovar P (1977) Acoustic emission of a cutting process. Ultrasonics 15:17–20
19. Vladisauskas A, Jakevicius L (2004) Absorption of ultrasonic waves in air. Ultragarsas 50(1):46–49
20. Urbikain G, Olvera D, Lopez de Lacalle L, Elias-Zuniga A (2015) Stability and vibrational behavior in turning processes with low rotational speeds. Int J Adv Manuf Technol 80:871–885
21. Kennametal. Products. [Online]. http://www.kennametal.com
22. Bruel and Kjaer. Products. [Online]. http://bksv.com/
23. MatWeb. (2016) MatWeb material property data. [Online]. http://www.matweb.com/
24. International Organization for Standardization (1961) Normal equal loudness contours and normal thresholds of hearing under free field listening conditions
25. Finnish Institute of Occupational Health (2011) Measurement of low frequency noise in rooms
26. Heinzel G, Rüdiger A, Schilling R (2002) Spectrum and spectral density estimation by the discrete Fourier transform (DFT), including a comprehensive list of window functions and some new flat-top windows
27. Unser M (2000) Sampling—50 years after Shannon. Proc IEEE 88: 569–587
28. Astakhov V (2005) On the inadequacy of the single-shear plane model of chip formation. Int J Mech Sci 47:1649–1672
29. Timoshemko S, Goodier J (1951) Theory of elasticity, 2nd edn. McGraw Hill, New York
30. Han S, Benoroya H, Wei T (1999) Dynamics of transversely vibrating beams using four engineering theories. J Sound Vib 225(5): 935–988
31. Cowper G (1966) The shear coefficient in Timoshenko's beam theory. J Appl Mech 33(2):335–340
32. Senkus A, Jotauiene E (2012) Investigation of vibro-acoustic properties of modern lathe collet chuck. J Vibroengineering 14(3):1227–1232

33. Tlusty J (1985) Handbook of high speed machining technology. Chapman and Hall, New York
34. Chung E, Chiou Y, Liang S (1994) Tool wear and chatter detection in turning via time series modeling and frequency band averaging. J Korean Soc Precis Eng 11(2):75–84
35. Seemuang N, McLeay T, Slatter T (2016) Using spindle noise to monitor tool wear in a turning process. J Adv Manuf Technol 86: 2781–2790
36. Takata S, Ahn J, Miki M, Miyao Y, Sata T (1986) A sound monitoring system for fault detection of machine and machining states. CIRP Ann Manuf Technol 35:289–292
37. Sata T, Takata S, Ahn J (1986) Operation monitoring of untended manufacturing systems by means of sound recognition. Model Sens Control Manuf Process PED:279–289
38. Ogata K (2001) Modern control engineering. Prentice Hall, Upper Saddle River